Fracture Analysis of S45C Medium Carbon Steel for the Van Front Drive Shaft

Yodnapha Ketmuang [1, *], Visanu Boonmag [2], and Aphinan Phukaoluan [3]

[1] Automotive Manufacturing Engineering, Faculty of Engineering and Technology, Panyapiwat Institute of Management, Bangkok 11120, Thailand
[2] Department of Mechanical Engineering, Faculty of Engineering, Thonburi University, Bangkok 10160, Thailand
[3] Department of Mechanical Engineering, Faculty of Engineering, Rajamangala University of Technology Krungthep, Bangkok 10120, Thailand
Email: Yodnaphaket@pim.ac.th (Y.K.); boonmagvisa@gmail.com (V.B.); aphinan.p@mail.rmutk.ac.th (A.P.)
*Corresponding author

***Abstract*—In this study, the drive shaft failure mode in a van is investigated by evaluation of the macroscopic and microscopic morphologies of the fracture surface, chemical composition, metallographic analysis, mechanical characteristics of the material, drive shaft fatigue test and finite element analysis. JIS-S45C hardened medium-alloyed steel was used to make the drive shaft. The failure mechanism for this drive shaft was mixed, which means that it was a combination of both brittle and ductile fractures. This is evident in the central interior region of the drive shaft. The summary result of this drive shaft fracture surface was that fatigue was the cause, and fatigue was the dominant mechanism of drive shaft failure due to obvious beach marks at the fracture surface and dimples at the central region. The shaft surface has a maximum hardness of 300 HV, while its centre axis has a minimum hardness of 214 HV. Additionally, the results of the R.R. Moore fatigue life assessment were compared with the outcomes of the numerical simulations performed using the ANSYS program. It was found from the fatigue experiment that the S-N Curve shows that fatigue life increases when the stress level acting on the test piece is reduced. It was discovered that the ANSYS assessment rate was a respectable 5% higher than the trial rate. The results of recommending materials used to make shafts for all 4 types found that the total deformation for AISI 5140 Steel is less when compared to the other three materials.**

***Keywords*—drive shaft, fatigue, numerical simulations**

I. Introduction

The drive shaft, a mechanical component of the transmission system, is used to transmit power from the engine to the wheels. It consists of two Constant Velocity (CV) joints, and Front Wheel Drive (FWD) vehicles nearly always use the shaft itself. The use of a drive shaft as a power transmitter in a car is more practical since chain-drives are more prone to breaking or jamming. The drive shaft often experiences torsional and bending stress during operation, which can lead to fatigue and fractural failures. Since drive shaft durability, as a crucial component of a vehicle, is a vital topic for engineers, several research studies based on the failure analysis, fracture mechanics, and fatigue strength of drive shafts have been performed. Oman Asi conducted a thorough analysis of the cause of fatigue failures, taking into account the literature review on failure analysis. The analysis revealed that critical regions where structural, material, or manufacturing defects are present are where fatigue failures typically begin to occur [1]. Tawancy *et al*. [2] investigate an automobile's failed rear axle shaft. As opposed to cleavage within the core, it was found that the cleavage occurred through an intergranular process. Although the precise chain of events leading to the fracture could not be traced, it is conceivable that it was started by a significant overload within the extremely hard and brittle case, which may have caused the vehicle to overturn, and that the final fracture was caused by the impact of overturning [2]. The shaft of a conveyor belt driving pulley failed in use, according to Zyl *et al.* [3]. To identify the contributing causes and circumstances of the failure, an investigation was carried out. It was determined that the shaft had worn out and that incorrect shaft reconditioning during normal maintenance had contributed to the failure [3]. According to research by Guimaraes *et al*. [4], a racing car gearbox system had an early breakdown after approximately 100 kilometres of operation. The results showed that the half-shaft alloy steel bar was not manufactured according to standard, resulting in lower strength and a material with insufficient loading capacity and fatigue resistance. Because of this, the half-shaft spline section exhibited a confluence of overload ductile fracture and torsional fatigue crack propagation during the fracture process [4]. The failure mode and root causes of a vehicle drive shaft are examined by Zhao *et al*. [5] They found that the root fillet's poor material quality, which is caused by relatively high manufacturing tolerances, also results in an increased stress concentration, which speeds up the beginning and growth of cracks [5]. The fracture failure analysis of the drive shaft was carried out by Liu *et al*. [6]

Manuscript received May 30, 2023; revised June 25, 2023; accepted August 11, 2023; published January 24, 2024.

They reached the conclusion that microscopic assessment of the fracture surface primarily showed dimples and a small degree of quasi-cleavage, which indicates that ductile fracture prevailed on the fracture surface. Several grey inclusions at the sample pit bottom have been identified as iron oxides by EDS spectrum analysis. Therefore, the presence of many iron oxide inclusions in the metal is certain to have a negative effect on the drive shaft's performance [6]. Maurya *et al*. [7] conducted the complete engineering failure analysis of the failed drive axle shaft of the material EN 24-T. In order to clarify the nature and cause of the failure, destructive testing, nondestructive testing, material analysis, and finite element simulations using ANSYS were also conducted. Failure analysis data points to errors in design considerations, and Scanning Electron Microscope (SEM) images reveal the formation of bainitic microstructures within the component as a result of insufficient heat treatment, reducing the material to a lower ultimate tensile strength [7]. The thread joint of a turbine shaft underwent fracture failure analysis and structural modification in the work of Liu *et al*. [6]. The microscopic study revealed that the fracture surface is mostly dispersed with a significant number of quasi-cleavages, suggesting that the material of the turbine shaft is mainly brittle. To improve the material, it is necessary to increase the susceptibility to bending, stress, and torsion. Additionally, it was found that the maximum stress value of the double-shoulder thread was lower than before the improvement. The research shows that structural design and material defects were the reason for the fracture of the turbine shaft joint [8].

These previously mentioned factors are often observed in earlier research. One of the most common events under normal operation, when the damaging stress is lower than the alternating stress, is fatigue. Shaft life is mostly based on the critical zone, where fatigue damage often begins when structural, material, and process defects are present. This research investigation attempts to identify the reasons behind the drive shaft failure in a 12-year-old van in which the engine was modified to provide increased horsepower. The information from the results of this investigation can help maintain and eliminate these shaft failures by identifying the damage mechanism.

II. Experimental Procedure

The experiment analyses can be divided into five methods through which the fracture at the failed drive shaft may have occurred. 1. Fracture surface analysis; 2. Material inspection; 3. Testing of the mechanical properties; 4. Fatigue test; 5. Modified drive shaft materials properties. The failure investigation's particular procedures were as follows.

A. Fracture Surface Analysis

Using a digital camera (Nikon D80), a visual examination of the failed drive shaft was performed to obtain a basic understanding of the fracture in terms of general characteristics and fracture surface. The fracture surface was subsequently investigated more closely via scanning electron microscope (JEOL: JSM-7800F prime). A drive shaft was used as the specimen, shown in Fig. 1.

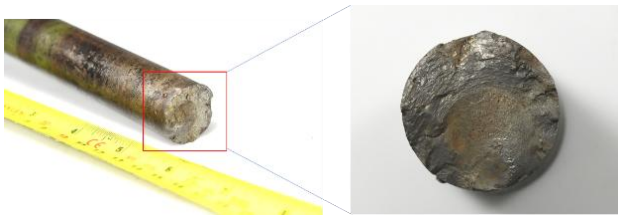

Fig. 1. Cutting position for macroscopic and microscopic examinations.

B. Material Inspection

A material inspection was performed to determine the metallographic structures and chemical compositions of the failed drive shaft material. An optical emission spectrometer (Thermo: ARL 3460) was used to investigate the chemical composition of the drive shaft material. The drive shaft material's transverse cross section was exposed to metallographic examinations, which were cold mounted using epoxy resin, polished using emery paper (down to #1200 grit), and polished with 1 μm diamond paste. After the etching process with 2% nital solution (2 mL HNO_3 + 100 mL DI water), the microstructure was examined using an optical microscope (OLS 4000 from Olympus).

C. Testing of the Mechanical Properties

For the mechanical properties test, assessing micro hardness, a hardness profile was prepared from the shaft surface through the central axis and aligned to the indentation to the other surface, on one side of the drive shaft within the surface area of the fracture surface, using an ANTON PAAR: MHT-10 with a diamond pyramid angle of 136˚ indenter and 300 g load.

D. Fatigue Test

In fatigue testing, the specimens are turned into 6 pieces with an 8 mm diameter and 90 mm length from failed drive shafts, as shown in Fig. 2. For the testing conditions, it should be noted that all fatigue tests are performed based on ISO standards]9[. The testing machine is composed of many fundamental components to which a number is assigned. Table I describes the numbered components of the R.R. Moore testing machine shown in Fig. 3. The test specimen has to be clamped at both ends, and then the constant test specimen is exposed to a load. The upper and lower surfaces of the specimen will be tensile and compressive, respectively, and the specimen will deflect. Then, the motor is turned until the specimen fractures. A digital revolution counter is required to record the number of revolutions until the failure happens, which is equivalent to the fatigue life of the shaft, whereupon a graph is created to show the relationship between stress and the number of cycles.

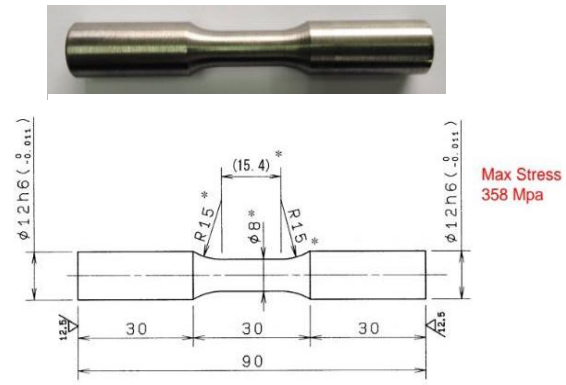

Fig. 2. Test specimen for fatigue.

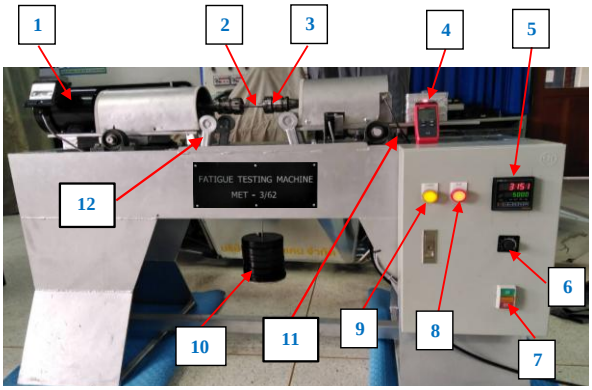

Fig. 3. Fatigue testing machine R.R. Moore.

TABLE I. CONSTITUTIVE COMPONENTS OF TESTING MACHINE

No.	Description	No.	Description
1	Electric Motor	7	On/Off Switch
2	Specimen	8	Start Light
3	Taper Fittings	9	Stop Light
4	Motor Tachometer	10	Standard Weight
5	Revolution Counter	11	Limit Switch
6	Variable Speed Drive	12	Holding Arm

E. Modified Drive Shaft Materials Properties

The drive shafts of the four materials were modelled according to the original dimensions of the shafts, and then they were assembled by Solidworks 2016 and the simulation was done by ANSYS Workbench 2020. Then 3-dimensional model can be seen in Fig. 4. For the stress analysis, we assume that the shafts are working in maximum load condition. In the van operation with transmission, the required power was taken as 130 kW and revolutions were 3800 rpm. The moment of force is considered in accordance with the van power and transmission ratios. The present objective is to use ANSYS as the solver to perform a finite element analysis of the drive shaft to determine the maximum bending stress. Drive shaft failure is caused by bending and torsional stress, which may contribute to fatigue and fracture failures.

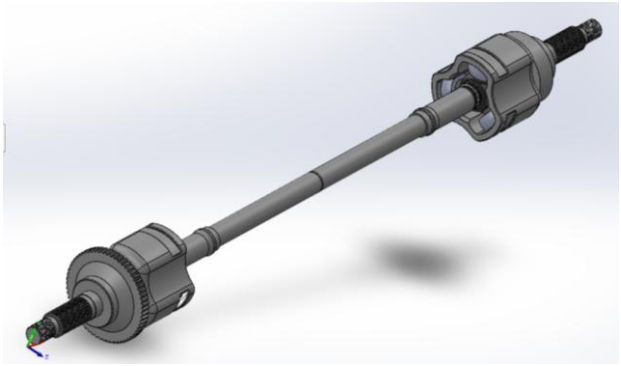

Fig. 4. Three-dimensional models of the drive shaft.

III. RESULTS AND DISCUSSION

A. Fracture Surface Analysis

Multiple crack sources were really initiated when low magnification drive shaft fracture surfaces were examined using a zoom stereo microscope, as shown in Fig. 5(a). During this slow crack growth, there were variations in the load that resulted in corresponding variations in the crack growth rate, which appear as beach marks confirming that the failure mode is a brittle fracture. The crack continues to grow slowly across the fatigue zone or areas that have been damaged by cyclic loads. The overload zone occurred when the crack eventually got to the point where the remaining material was under stress. An expanded view of the origin of the crack is shown in Fig. 5(b). Consider the examination in the image and compare it with the fatigue crack in Fig. 6. It was found by examination of the schematic diagram that reversed bending was the problem [10–15].

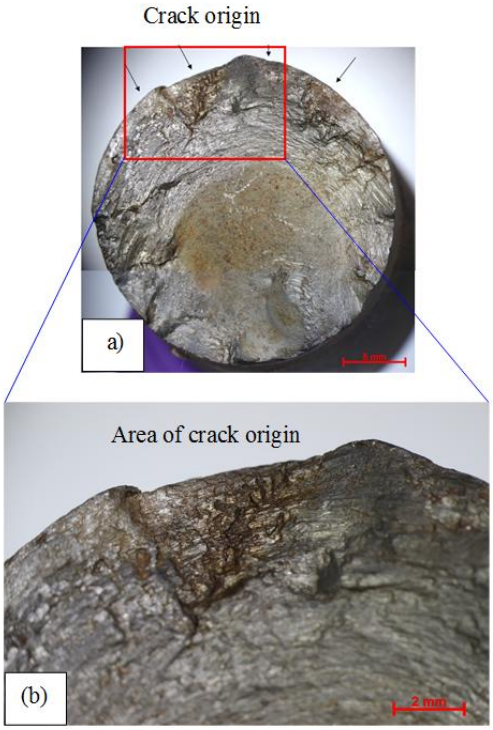

Fig. 5. The drive shaft's fracture characteristics as a result of fatigue.

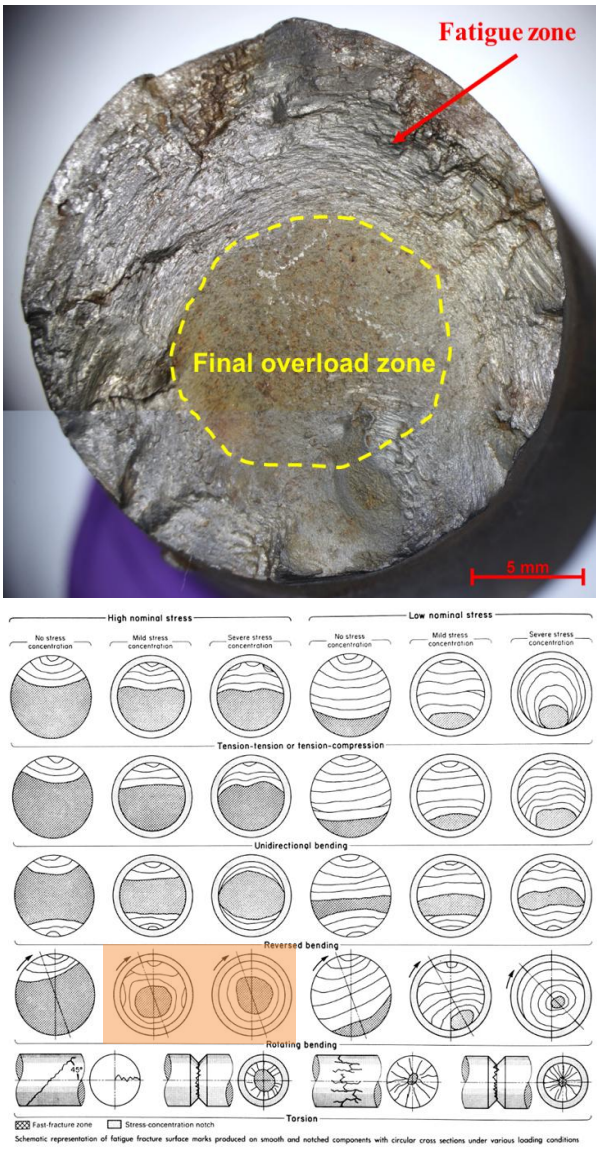

Fig. 6. Fracture images and schematic diagrams of fatigue fractures can be obtained from ASM Metals Handbook.

A scanning electron microscope was used to examine the surface layer cracking. Fig. 7(a) exhibits an image of the center region fracture. Dimples are clearly apparent from the same point in Fig. 7(b) when it is magnified; this structure is characteristic of a fracture followed by uniaxial tensile failure. Each dimple is one half of a microvoid that forms during the fracture process and is subsequently cracked separately. In the situation of a fracture, dimples appear on the 45-degree shear lip. The fracture form of the ductile, which results from shear behavior, is elongated or C-shaped, and this parabolic shape may be characteristic of shear failure [16].

Fig. 8 shows a surface layer examination of the crack origin in Area 1. SEM was used in Area 1 to analyze the chemical composition of the fracture surfaces of the drive shaft for inclusions using Energy Dispersive Spectroscopy (EDS). The line of scan shows that the majority of the elements within the standard percentage by weight of the steel material are iron (Fe), Carbon (C), and Oxygen (O). The drive shaft alloy composition was confirmed to be medium alloy S45C with no abnormalities.

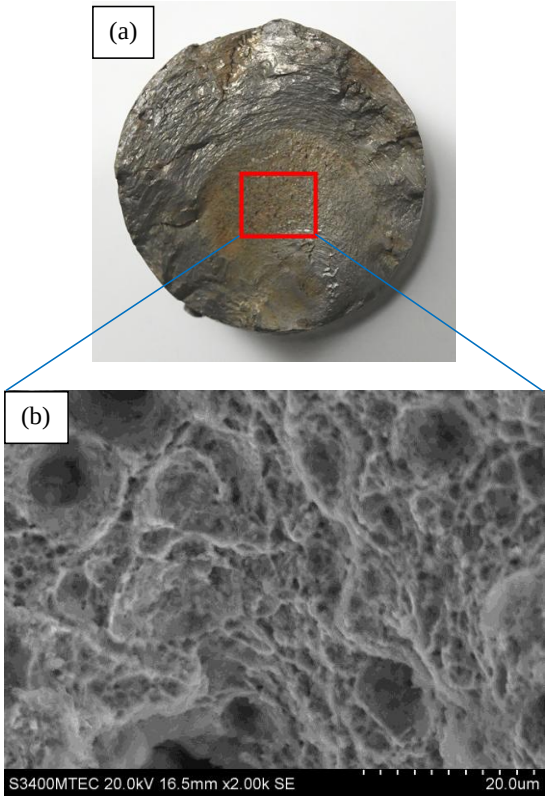

Fig. 7. SEM micrograph. (a) The central region fracture. (b) The enlarged image of the crack area showing the appearance of a hole in the crack (dimples) at a magnification of 2kx, 20 μm.

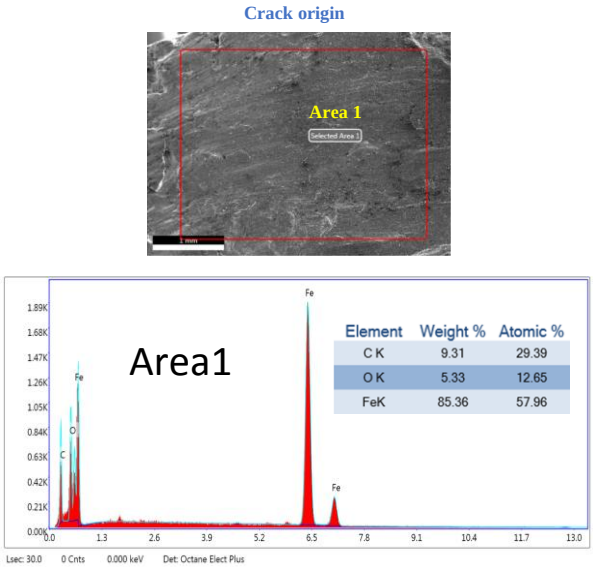

Fig. 8. Results from the EDS on the Area 1 crack origin.

Fig. 9 shows an inspection of the surface layer on the final overload zone in Areas 1, 2, and 3. SEM was used to analyze the chemical composition of the fracture surfaces using energy dispersive Spectroscopy (EDS) for inclusions at the drive shaft fracture surface in Areas 1, 2, and 3. The line of scan shows that most of the elements within the standard percentage by weight of the steel

material are iron (Fe), Carbon (C), Silicon (Si), and Oxygen (O). The drive shaft composition was confirmed to be medium alloy S45C with no abnormalities [17].

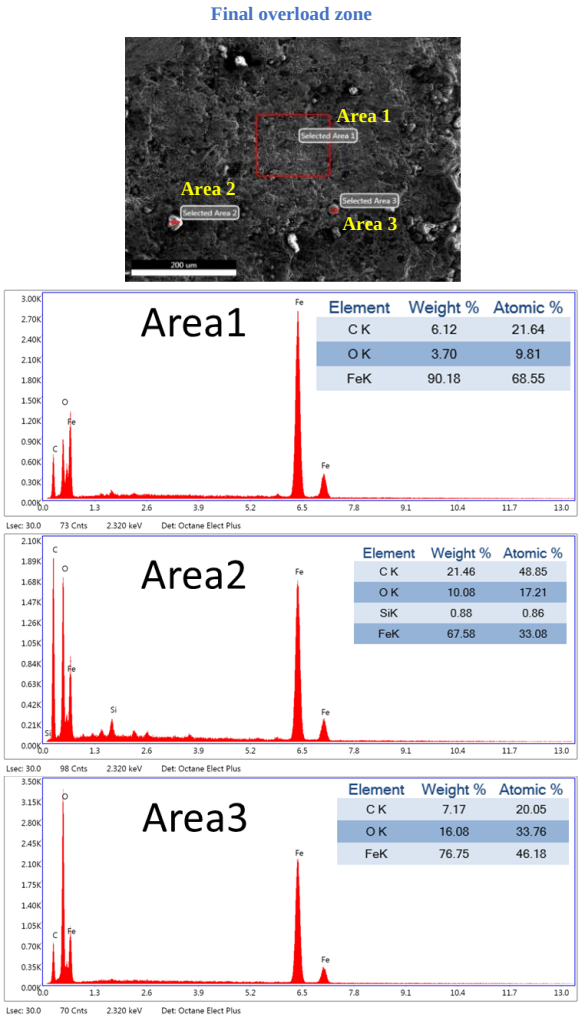

Fig. 9. The EDS results on the final overload zone from Areas 1, 2 and 3.

B. Material Inspection

A spectrophotometer test machine was used to examine the chemical composition of the shaft material. Table II shows the average chemical composition values for the shaft material. The medium-alloyed steels JIS G4051: Standard grade S45C, commonly and widely used in making shafts. This means that proper material was used for making the shafts [18].

Metallographic examinations were also carried out. An optical microscope was used to polish, etch, and photograph a transverse cross section of the failing drive shaft. Tempered martensite consists of the microstructure of the outer peripheral region, shown in Fig. 10 [19]. However, ferrite and pearlite formed the microstructure in the central region, as shown in Fig. 11. The heat treatment condition of the shaft was induction hardened, quenched, and tempered, which is standard procedure for the heat treatment of S45C steel, according to the microstructure.

TABLE II. CHEMICAL COMPOSITION OF THE FAILED DRIVE SHAFT AND THAT OF S45C STEEL (%WT)

Materials	Failed drive shaft	SCM418
C	0.47	0.42-0.48
Si	0.19	0.15-0.35
Mn	0.78	0.60-0.90
P	0.013	≤0.030
S	0.018	≤0.035
Ni	0.02	≤0.20
Cr	0.18	≤0.20
Cu	0.01	≤0.30

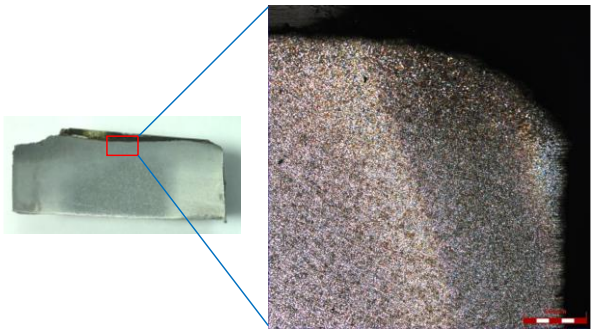

Fig. 10. Optical photomicrograph of the failing drive shaft outside the perimeter region, which is composed of tempered martensite, 50x, 500 μm.

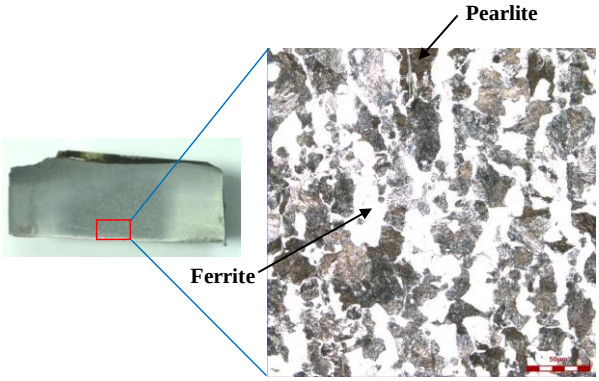

Fig. 11. Optical photomicrograph of the pearlite- and ferrite-containing concentrate region of the failing drive shaft, 50x, 500 μm.

C. Testing of the Mechanical Properties

Additionally, as shown in Fig. 12, microhardness examinations are performed by pressing the cross-sectional initial to the outer surface of the shaft through the center axis, oriented in the direction of pressing to the other surface of the drive shaft. Fig. 13 shows the results of the hardness measurements. The surface hardness at the initial position was 275 HV (26.5 HRC), then it decreased radially to reach the lowest value in the shaft at the centre, which was 214 HV (16 HRC), before reaching the hardness value of 300 HV (30 HRC). It was proposed that the axle underwent induction hardening based on the observed microstructures and this hardness profile [20].

Fig. 12. The failed drive shaft hardness measurement line is measured from the case to the core of the shaft.

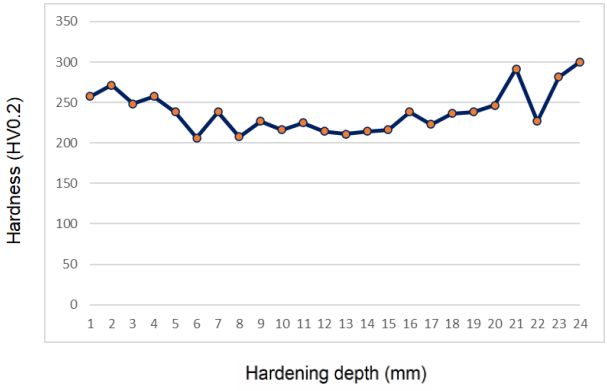

Fig. 13. The graph shows the hardness layer of the failed drive shaft.

D. Fatigue Test

The tensile strength and yield strength of the medium carbon steel S45C shaft material is 569 MPa and 343 MPa, respectively [21]. The loading frequency was 50 Hz, which was a motor speed of 1725 rpm. All fatigue tests were carried out at an ambient temperature of 25 ℃. The applied loads for stress levels were considered as 150, 145, 140, 135, 130, and 125 N, respectively. The specimen for the fatigue test is shown in Fig. 14 and was made of medium carbon steel S45C that was obtained from a failed drive shaft. This method was carried out in parallel with numerical simulations of the test specimens using the ANSYS software; stress values for Von Mises stress and endurance limits were obtained from the simulations with a load of 150 N, as shown in Figs. 15 (a)–(b), respectively [22].

The results of the experimental fatigue life of the shaft material under a cyclic load of S45C steel will be tested for all 6 pieces; the values are shown in Table III and can be drawn on the S-N curve as shown in Fig. 16. These results can then be compared with the results of numerical simulations performed using the ANSYS program. It appears that ANSYS had an assessment rate that was approximately 5% higher than that of the trial. It remains a consideration that the graph had a downward curve [23]. Weight reductions of 5 N were made to the weight in each trial. It was discovered that the 125 N weight produced the highest number of cycles (947,346) and the 150 N weight produced the lowest number of cycles (285,962). According to the results of the experiment, the life of the test piece increases according to the S-N curve when the stress level acting upon it is decreased to a less fatigued level. The summary result of the S-N curve is consistent with the situations before and after the increase of engine power which affects the failure of the drive shaft, by observing the crack origin occurring at the outer surface of the shaft until the crack expands along the beach marks towards the final overload zone at the central axis of the specimen as shown in Fig. 17. Before adjusting the engine power to be comparable to the low weight applied to the specimen, there will be high numbers of cycles in the failed specimen. After adjusting the engine power to a comparable increase in the weight applied to the specimen, there will be a low number of cycles in the failed specimen [24].

Fig. 14. S45C steel was used for fatigue testing before and after the experiment.

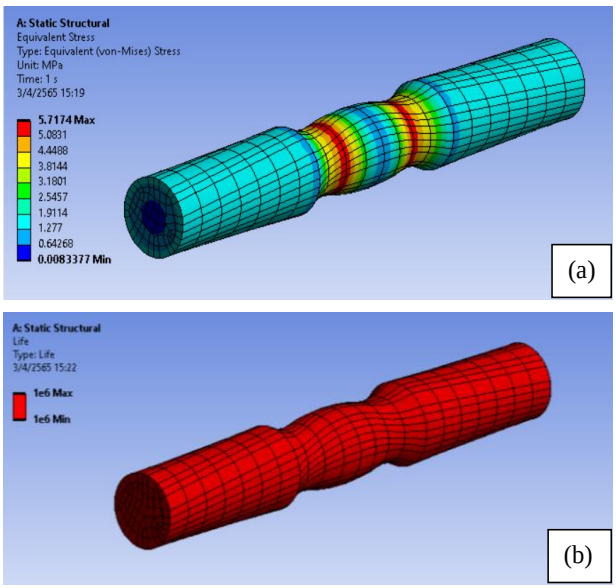

Fig. 15. The numerical simulations of the test specimens using the ANSYS software. (a) Von Mises stress results and (b) Endurance limits with a load of 150 N.

TABLE III. COMPARISON OF FATIGUE LIFE BETWEEN THE R.R. MOORE FATIGUE TESTING MACHINE AND ANSYS

Load (N)	Number of cycles (N)	
	Fatigue test	ANSYS
125	947,346	1,000,000
130	693,212	7.28×10^5
135	582,186	6.11×10^5
140	447,470	4.70×10^5
145	352,080	3.70×10^5
150	285,962	3.01×10^5

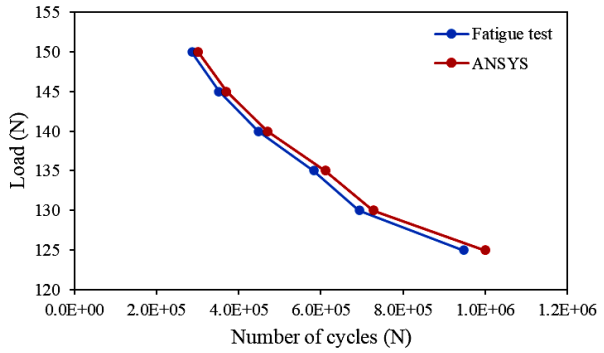

Fig. 16. Comparison of fatigue life chart from the fatigue test and finite element methods (ANSYS).

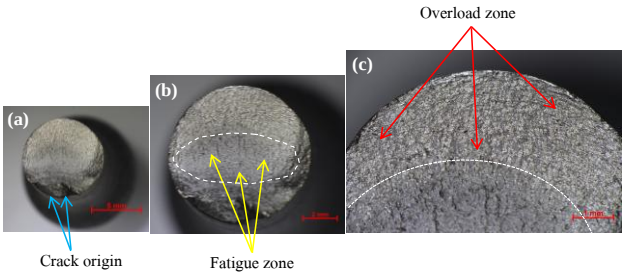

Fig. 17. Fracture characteristics photographs of specimens with Zoom Stereo Microscope.

E. Modified Drive Shaft Materials Properties

For each of the four materials used for creating the drive shaft, an investigation was performed. Drive shaft failure is caused by torsional stress, which may contribute to fatigue and fracture failures. To minimize drive shaft failure and improve the design, stress analysis is a key area of research. For the shaft design, it is important to analyze the torsional stress that develops between the matching driving shafts. The present objective is to use ANSYS as the solver to perform a finite element analysis of the drive shaft to determine the maximum torque. Table IV compares the various qualities of the 4 materials so that the relevance for usage in this case study can be assessed [25–27].

The maximum torque of the drive shaft was calculated based on power taken as 130 kW and revolutions of 3800 rpm using the following Eq. (1):

$$T = \frac{P60}{2\pi N} \tag{1}$$

$$T = \frac{130\times10^{3}\times60}{2\pi\times3800} = 327 \text{ N-m}$$

The structural analysis of the drive shafts model is carried out using the finite element analysis in ANSYS Workbench 2020. The boundary condition was applied to the torque which was set into the drive shaft at 327 N-m. The mesh was generated with tetrahedral elements. The generated mesh operation models have 60,395 total elements and 87,575 total nodes. Degrees of Freedom (DOF) were selected for mesh control x, y, and z axes only [26]. By applying the analysis to the drive shaft that is subjected to torque, the numerical stress distributions are then obtained and imported into the ANSYS Workbench program. Fig. 18 shows the Von Mises stress distribution plot along the drive shaft from material AISI 1045 from the simulations with a torque of 327 N-m. Fig. 19 shows total deformation with a torque of 327 N-m. Fig. 20 shows the safety factor min obtained from material AISI 1045 from the simulations with a torque of 327 N-m and the data from Table V show that material AISI 5140 has the highest safety values compared to the other three materials.

TABLE IV. COMPARISON OF THE 4 MATERIALS AND PROPERTIES

Materials	Yield strength (σ_y) MPa	Modulus of elasticity (E) GPa	Poisson's Ratio
AISI 5140	295	190	0.27
AISI 1045	310	200	0.29
AISI 1080	370	205	0.29
AISI 9310	440	210	0.30

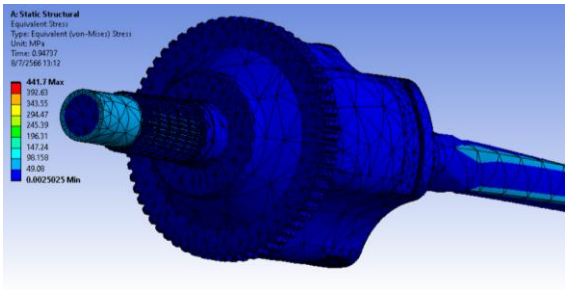

Fig. 18. Von Mise's stress with a torque of 327 N-m.

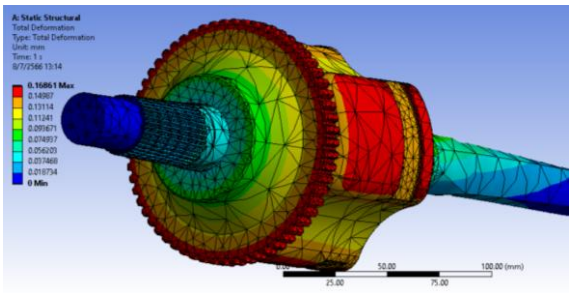

Fig. 19. Total deformation with a torque of 327 N-m.

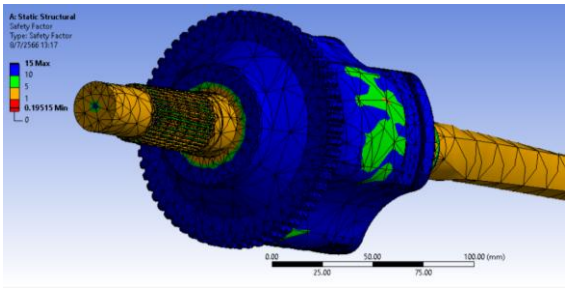

Fig. 20. Safety factor min with a torque of 327 N-m.

From Table V, it can be considered that for the drive shaft to have a basic design, the stress of the material yields approximately the same value for all four materials. However, total deformation for material AISI 5140 is less

when compared to the other three different materials, including AISI 1045 Carbon, AISI 1080 Steel, and AISI 9310 Steel [27].

TABLE V. RESULTS OF THE 4 MATERIALS

Materials	Stress (σ_a) MPa	Total Deformation ($\mathcal{E}$) mm	Safety Factor Min.
AISI 5140	439	0.16758	0.19635
AISI 1045	441.7	0.16861	0.19515
AISI 1080	444.41	0.16964	0.19397
AISI 9310	447.11	0.17067	0.19279

IV. CONCLUSIONS

The critical zone of the shaft surface is the origin of the crack due to fatigue fracture, which allows high stresses to cause cracking and expands the crack growth rate which appears as beach marks, whereby the mode is brittle fracture. The final fracture in the central axis exhibits dimples; this type of fracture indicates a shear failure in the ductile fracture mode. Drive shaft microstructures appeared to consist of tempered martensite in the surface area and a ferrite alloy mixed with pearlite in the central axis. The drive shaft in the centre was determined to contain the lowest hardness for radial hardness at 16 HRC, while the highest hardness, 30 HRC, was recorded close to the surface. It was considered that the axle had been induction hardened based on the observation of the microstructure and the result of the hardness value. The S-N graph has a downward curving trend. The results showed that the weight of 125 N provided the highest number of cycles counted (947,346) and the weight of 150 N provided the lowest number of cycles counted (285,962). According to the S-N curve, test piece fatigue life is enhanced with fewer test pieces. The results of the numerical simulations performed using the ANSYS program were compared to the results of the R.R. Moore fatigue life assessment. It was found that the ANSYS assessment rate was an appropriate 5% higher than the trial rate. In comparing the materials used to make all 4 types of drive shafts, it was found that the base design developed from AISI 5140 material yields less total deformation than the other three materials.

CONFLICT OF INTEREST

The authors declare no conflict of interest.

AUTHOR CONTRIBUTIONS

Visanu Boonmag contributed to this research by implementing the experimental and analytical work with the guidance and supervision from Aphinan Phukaoluan and Yodnapha Ketmuang; all authors had approved the final version.

ACKNOWLEDGMENTS

For research equipment and facilities, Automotive Manufacturing Engineering, Faculty of Engineering and Technology, Panyapiwat Institute of Management supported the research. The authors express thanks to the National Metal and Materials Technology Center (MTEC) for providing help and guidance during the research process. Additionally, the authors are thankful for the accessibility of Solidworks 2016 and ANSYS Workbench 2020 for the simulation by the Department of Mechanical Engineering, School of Engineering, King Mongkut's Institute of Technology Ladkrabang.

REFERENCES

[1] O. Asi, "Fatigue failure of a rear axle shaft of an automobile," *Engineering Failure Analysis*, vol. 13, no. 8, pp. 1293–1302, 2006.
[2] H. M. Tawancy and Luai M. Al-Hadhrami, "Failure of a Rear Axle Shaft of an Automobile Due to Improper Heat Treatment," *Journal of Failure Analysis and Prevention*, vol. 13, no. 2, pp. 353–358, 2013.
[3] G. V. Zyl and A. Al-Sahli, "Failure analysis of conveyor pulley shaft," *Case Studies in Engineering Failure Analysis*, vol. 1, no. 2, pp. 144–155, 2013.
[4] A.V. Guimaraes, P.C. Brasileiro, G.C. Giovanni, L.R.O. Costa and L.S. Araujo, "Failure analysis of a half-shaft of a formula SAE racing car," *Case Studies in Engineering Failure Analysis*, vol. 7, pp. 17–23, 2016.
[5] L. H. Zhao, Q. K. Xing, J. Y. Wang, S. L. Li and S. L. Zheng, "Failure and root cause analysis of vehicle drive shaft," *Engineering Failure Analysis*, vol. 99, pp. 225–234, 2019
[6] Y. Liu, Z. Lian, C. Xia, L. Qian and S. Liu, "Fracture failure analysis and research on drive shaft of positive displacement motor," *Engineering Failure Analysis*, vol. 106, 2019.
[7] P. Maurya, N. Mulani, C. Michael and D. Jebaseelan, "Failure Analysis of Drive Axle Shaft failed under Torsional Stress," *Materials Science and Engineering*, vol. 1128, 2021
[8] Y. Liu, Z. Lian, S. Liu and T. Luo, "Fracture failure analysis and structure improvement on thread joint of turbine shaft," *Engineering Failure Analysis*, vol. 115, 2020.
[9] Metallic materials - Rotating bar bending fatigue testing, Standard No. ISO 1143, ISO International Standard, 2010.
[10] C. K. Clarke and D. Halimunanda, "Failure Analysis of Induction Hardened Automotive Axles," *Journal of Failure Analysis and Prevention*, vol. 8, no.4, pp. 386–396, 2008.
[11] S. Das, G. Mukhopadhyay and S. Bhattacharyya, "Failure analysis of axle shaft of a fork lift," *Case Studies in Engineering Failure Analysis*, vol. 3, pp. 46–51, 2015.
[12] S. D. Dalvi, H. D. Chandrababu, S. Satav and Vijoykumar, "Failure analysis of a carbon steel roller shaft of continuous pad steam machine," *Case Studies in Engineering Failure Analysis*, vol. 9, pp. 118–128, 2017.
[13] C. Moolwan and S. Netpu, "Fatigue failure of an idle gear shaft of a gearbox," *Materials Science and Engineering*, vol. 501, no. 1, 2019.
[14] A. Roy, P. Palita, S. Das and G. Mukhyopadyay, "Investigation of torsional fatigue failure of a centrifugal pump shaft," *Engineering Failure Analysis*, vol. 112, 2020.
[15] V. Giannella, R. Sepe, A. Borrelli, G. De Michele, E. Armentani, "Numerical investigation on the fracture failure of a railway axle", *Engineering Failure Analysis*, vol. 129, 2021.
[16] T. F. Azevedo, W. R. Viana Sampaio, E. César Bezerra Câmara, G. Dória Lima, W. Franklin dos Santos Silva and Simone da Silva Ramos, "Failure analysis of a sugarcane loader rear shaft," *Engineering Failure Analysis*, vol. 109, 2020.
[17] R. S. Miranda, C. Cruz, N. Cheung and Adilto P. A. Cunha, "Fatigue Failure Analysis of a Speed Reduction Shaft," *Metals*, vol. 11, no. 6, pp. 856, 2021.
[18] Carbon steels for machine structural use, Japanese industrial standard (JIS G 4051), 2016.
[19] M. Banuta and I. Tarquini, "Fatigue Failure of a Drive Shaft," *Journal of Failure Analysis and Prevention*, vol. 12, no. 2, pp. 139–144, 2012.
[20] S. Cai, J. Sun, Q. He, T. Shi, D. Wang, J. Si, J. Yang, F. Li, K. Xie, and M. Li, "16MnCr5 gear shaft fracture caused by inclusions and heat treatment process," *Engineering Failure Analysis*, vol. 126, 2021.

[21] R. Karimbaev, S. Choi, Y. S. Pyun, and A. Amanov, "Mechanical and tribological characteristics of cladded AISI 1045 carbon steel," *Materials*, vol. 13, pp. 859, 2020.
[22] A. M. Eleiche, M. M. Megahed, and N. M. Abd-Allah, "Low-cycle fatigue in rotating cantilever under bending. III: Experimental investigations on notched specimens," *International Journal of Fatigue*, vol. 28, pp. 271–280, 2016.
[23] S. Seifoori, A. M. Parrany, and M. Khodayari, "A high-cycle fatigue failure analysis for the turbocharger shaft of BELAZ 75131 mining dump truck," *Engineering Failure Analysis*, vol. 116, 2020.
[24] M. J. Khameneh and M. Azadi, "Evaluation of high-cycle bending fatigue and fracture behaviors in EN-GJS700-2 ductile cast iron of crankshafts," *Engineering Failure Analysis*, vol. 85, pp. 189–200, 2018.
[25] A. K. Ahmed, S. Y. Ezdeen, and A. M. Sinjari, "Analyzing the stress and modal behavior of a reconfigurable gripper's finger with different fabrication materials," *International Journal of Mechanical Engineering and Robotics Research*, vol. 11, no. 11, pp. 820–833, 2022.
[26] V. Boonmag, A. Phukaoluan, O. Wisesook, and G. Pluphrach, "Comparison of Bending Stress and Contact Stress of Helical Gear Transmission Using Finite Element Method," *International Journal of Mechanical Engineering and Robotics Research*, vol. 8, no. 1, pp. 99–103, 2019.
[27] P. Kulkarni, H. Yaragudri, and U. Farooq M A, "Contact Stress Analysis and Optimization of Bevel Gear Pairs by Theoretical and FEA," *International Journal of Latest Technology in Engineering, Management & Applied Science (IJLTEMAS)*. vol. 4, pp. 2278–2540, 2017.